

Electronic Supplementary Information for

Visible-Light-Sensitive Water Splitting Photocatalyst Composed of Rh<sup>3+</sup> in a 4d<sup>6</sup> Electronic Configuration, Rh<sup>3+</sup>-Doped ZnGa<sub>2</sub>O<sub>4</sub>

Naoya Kumagai,<sup>a</sup> Lei Ni<sup>b</sup> and Hiroshi Irie\*<sup>b,c</sup>

<sup>a</sup> Graduate School of Engineering, University of Yamanashi, 4-3-11 Takeda, Kofu, Yamanashi 400-8511, Japan  
<sup>b</sup> Clean Energy Research Center, University of Yamanashi, 4-3-11 Takeda, Kofu, Yamanashi 400-8511, Japan. Fax: +81 55 220 8092; Tel: +81 55 220 8092; E-mail: hirie@yamanashi.ac.jp  
<sup>c</sup> Japan Science and Technology Agency, CREST, 5 Sanbancho, Chiyoda-ku, Tokyo 102-0075, Japan

Contents

- ESI-1) Schematic illustration of ligand-field splitting of an octahedrally coordinated Rh<sup>3+</sup> (Fig. S1)
- ESI-2) Changes in O<sub>2</sub> concentration of Rh<sub>2</sub>O<sub>3</sub>/ZRO in the presence of AgNO<sub>3</sub> (Fig. S2)
- ESI-3) Additional explanations for the band structure of ZGO
- ESI-4) Density of states (DOS) calculation
- ESI-5) Experimental details
- ESI-6) Detailed characterizations, ICP-AES, and X-ray diffraction profiles of ZGRO and Rh<sub>2</sub>O<sub>3</sub>/ZGRO (Fig. S3), and SEM images of ZGRO and Rh<sub>2</sub>O<sub>3</sub>/ZGRO (Fig. S4)
- ESI-7) Additional explanations for the band structure of ZGRO
- ESI-8) Wavelength distribution of the irradiated light (Fig. S5)
- ESI-9) Additional explanation for the H<sub>2</sub> evolution activity in the presence of Rh<sub>2</sub>O<sub>3</sub>/ZGRO
- ESI-10) Details for the estimation of the turnover number
- ESI-11) Preliminary experiments for the H<sub>2</sub> evolution in the presence of photocatalysts obtained by the solid state reaction (Fig. S6 and Fig. S7)

**ESI-1) Schematic illustration of ligand-field splitting of an octahedrally coordinated Rh<sup>3+</sup> (Fig. S1)**

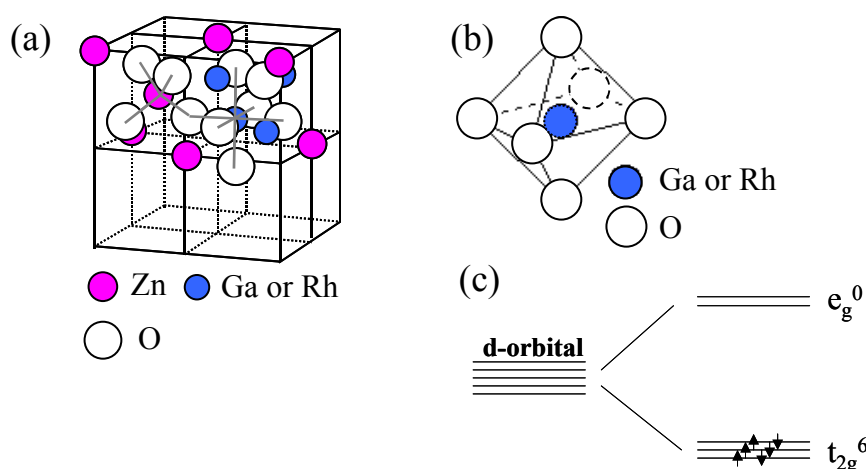


Figure S1. (a) Crystal structure of spinel  $\text{ZnGa}_2\text{O}_4$  or  $\text{ZnRh}_2\text{O}_4$ . (b)  $\text{ZnGa}_2\text{O}_4$  and  $\text{ZnRh}_2\text{O}_4$  have  $\text{Ga}^{3+}$  and  $\text{Rh}^{3+}$  ions, respectively, in a regular octahedral coordination. (c) In this coordination, the  $\text{Rh}^{3+}$  ( $\text{Rh} \text{d}^6$ ) forms fully occupied  $t_{2g}^6$  and empty  $e_g^0$  sets as a result of ligand-field splitting of an octahedrally coordinated  $\text{Rh}^{3+}$ .

**ESI-2) Changes in O<sub>2</sub> concentration of Rh<sub>2</sub>O<sub>3</sub>/ZRO in the presence of AgNO<sub>3</sub> (Fig. S2)**

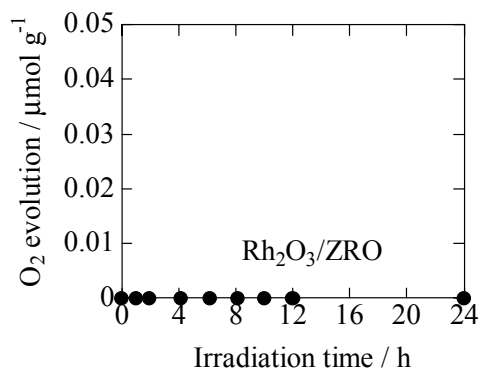


Figure S2. Changes in  $\text{O}_2$  concentration by water splitting as a function of time in the presence of  $\text{Rh}_2\text{O}_3/\text{ZRO}$  (see ESI-5) photocatalyst under visible-light irradiation at  $> 420$  nm.  $\text{AgNO}_3$  was added as sacrificial agent.  $\text{O}_2$  evolution was not observed at all.

**ESI-3) Additional explanations for the band structure of ZGO**

According to Ikarashi *et al.* (ref. 9), the character of valence band in  $\text{ZnGa}_2\text{O}_4$  is the same as that in metal oxides whose valence band are composed of O 2p. In addition, according to Scaife (*Solar Energy*, 1980, **25**, 41-54), the VB top potential of a typical oxide, whose VB is mainly composed of O 2p is 2.94 V (vs. SHE). Thus, we consider that the VB top of  $\text{ZnGa}_2\text{O}_4$  is approximately 3 V.

**ESI-4) Density of states (DOS) calculation**

The plane-wave-based density functional method for the DOS calculation was performed within the generalized gradient approximation using the ab initio total-energy and molecular dynamics program VASP (Vienna Ab initio Simulation Program) (refs. (a) Kresse, G.; Hafner, J.; *Phys. Rev. B*, 1993, **48**, 13115-13118. (b) Kresse, G.; Furthmüller, J.; *Phys. Rev. B*, 1996, **54**, 11169-11186). The core orbitals were replaced by ultrasoft pseudopotentials with a kinetic energy cutoff of 500 eV. The compositions used for the calculation were  $\text{ZnGa}_2\text{O}_4$  ( $\text{Zn}_2\text{Ga}_4\text{O}_8$  cell) (a) and  $\text{Zn}(\text{Ga}_{1-x}\text{Rh}_x)_2\text{O}_4$  ( $x = 0.25$ ) ( $\text{Zn}_2\text{Ga}_3\text{RhO}_8$  cell). The cubic spinel phase was adopted for the calculation.

### ESI-5) Experimental details

The crystal structures of the prepared powders were identified by X-ray diffraction (XRD) (Panalytical PW-1700). Elemental analysis of the prepared photocatalysts (ZGRO and Rh<sub>2</sub>O<sub>3</sub>-grafted ZGRO) was performed using an inductively coupled plasma atomic emission spectrometer (ICP-AES) (SPS1700, Seiko Instruments Inc.) for Zn, Ga, and Rh. The morphology of the Rh<sub>2</sub>O<sub>3</sub>-grafted sample was investigated by field emission scanning electron microscopy (SEM) (S-4500, Hitachi). Brunauer–Emmett–Teller (BET) surface areas were determined using a nitrogen adsorption apparatus (Micromeritics, TriStar 3000, Shimadzu). UV-visible absorption spectra were obtained by the diffuse reflection method using a spectrometer (V-650, JASCO).

Photocatalytic reactions were performed in a gas-closed-circulation system. Bare or Rh<sub>2</sub>O<sub>3</sub>-grafted ZGRO powders (60 mg) with either CH<sub>3</sub>OH or AgNO<sub>3</sub> as sacrificial agents were suspended in water (10 ml) at pH 7 using a magnetic stirrer. Argon gas (50 kPa) was introduced into the system after deaeration. A Xe lamp (LA-251Xe, Hayashi Tokei) equipped with a glass filter (either Y-44 or Y-52, Asahi Techno-glass) was employed for visible light irradiation with wavelengths of > 420 and > 500 nm, respectively. The amounts of evolved H<sub>2</sub> and O<sub>2</sub> were monitored using an online gas chromatograph (GC-8A, Shimadzu).

For reference samples, the Zn(Ga<sub>1-x</sub>Rh<sub>x</sub>)<sub>2</sub>O<sub>4</sub> powders ( $x = 0, 1$ ), i.e., ZnGa<sub>2</sub>O<sub>4</sub> and ZnRh<sub>2</sub>O<sub>4</sub> (designated as ZGO and ZRO, respectively, the same in Fig. 1), were synthesized using a solid state reaction. Commercial ZnO (Wako), Ga<sub>2</sub>O<sub>3</sub> (Wako), and Rh<sub>2</sub>O<sub>3</sub> (Wako) powders were used as starting materials. Stoichiometric amounts of the starting materials for ZGO and ZRO were wet ball-milled for 16–20 h using ZrO<sub>2</sub> balls as the milling medium in polyethylene bottles. The resulting mixtures for ZGO and ZRO were pressed into pellets, calcined at 1000 °C for 24 h, and then thoroughly ground. In addition, Zn(Ga<sub>1-x</sub>Rh<sub>x</sub>)<sub>2</sub>O<sub>4</sub> ( $x = 0.02$ ) powders were synthesized by using the obtained ZGO and ZRO powders. These powders were again wet ball milled for 16–20 h in ratios corresponding to the compositions of Zn(Ga<sub>1-x</sub>Rh<sub>x</sub>)<sub>2</sub>O<sub>4</sub> ( $x = 0.02$ ). The powders were pressed into pellets, heated at 1000°C for 24 h, and thoroughly ground. Then, we obtained solid-state-reacted Zn(Ga<sub>1-x</sub>Rh<sub>x</sub>)<sub>2</sub>O<sub>4</sub> ( $x = 0.02$ ) powders, designated as ZGRO (SSR), being distinguished from merely “ZGRO” obtained by the hydrothermal method in the main text and ESI. The graft of Rh<sub>2</sub>O<sub>3</sub> as a co-catalyst onto ZGRO (SSR), ZnGa<sub>2</sub>O<sub>4</sub> and ZnRh<sub>2</sub>O<sub>4</sub> (0.5 wt% of Rh<sub>2</sub>O<sub>3</sub> relative to ZGRO (SSR), ZGO and ZRO) was performed by the same impregnation method described in the main text.

We performed the preliminary experiments to evaluate the H<sub>2</sub> evolutions in the presence of Rh<sub>2</sub>O<sub>3</sub>/ZGRO (SSR), Rh<sub>2</sub>O<sub>3</sub>/ZGO and Rh<sub>2</sub>O<sub>3</sub>/ZRO in the presence of CH<sub>3</sub>OH under visible light irradiation with the wavelength of > 420 nm. The results are described in ESI-10.

### ESI-6) Detailed characterizations, ICP-AES, and X-ray diffraction profiles of ZGRO and Rh<sub>2</sub>O<sub>3</sub>/ZGRO (Fig. S3), and SEM images of ZGRO and Rh<sub>2</sub>O<sub>3</sub>/ZGRO (Fig. S4)

Elemental analysis by ICP-AES indicated that the molar ratio of Zn:Ga:Rh in the bare ZGRO was 0.77:1.95:0.05 (the starting ratio used in the preparation was 1:1.96:0.04). We also applied ICP-AES to the analysis of Rh<sub>2</sub>O<sub>3</sub>/ZGRO. As the loaded amount of Rh<sub>2</sub>O<sub>3</sub> was very small (0.5 wt% vs. ZGRO, the molar ratio of Rh in Rh<sub>2</sub>O<sub>3</sub> to Rh in ZGRO was 0.011 in the starting ratio), we could not detect the exact amount of loaded Rh in Rh<sub>2</sub>O<sub>3</sub>/ZGRO due to the specifications of the apparatus. This means that the difference in the amounts of Rh between in ZGRO and in Rh<sub>2</sub>O<sub>3</sub>/ZGRO is so small that we could not detect the exact amount of loaded Rh in Rh<sub>2</sub>O<sub>3</sub>/ZGRO. However, based on our experiences with this type of analysis, it is likely that the actual weight fraction of Rh<sub>2</sub>O<sub>3</sub> relative to ZGRO was 0.005 (0.5 wt%).

The XRD patterns of the as-prepared ZGRO and Rh<sub>2</sub>O<sub>3</sub>/ZGRO powders indicated they adopted a cubic crystal structure with a spinel crystalline phase (Fig. S3). The peaks originating from grafted Rh<sub>2</sub>O<sub>3</sub> were not observed in the presence of Rh<sub>2</sub>O<sub>3</sub>/ZGRO due to the small amount of Rh<sub>2</sub>O<sub>3</sub> present (0.5 wt% of Rh<sub>2</sub>O<sub>3</sub> relative to ZGRO, starting ratio). The peaks of Rh<sub>2</sub>O<sub>3</sub>/ZGRO were sharper than those of the as-prepared ZGRO because ZGRO in Rh<sub>2</sub>O<sub>3</sub>/ZGRO was calcined at 500 °C for 1 h during the grafting procedure of Rh<sub>2</sub>O<sub>3</sub>.

The crystallite sizes of as-prepared ZGRO and Rh<sub>2</sub>O<sub>3</sub>/ZGRO were ranged from 15 to 30 and 30 to 50 nm, respectively (Fig. S4). It is quite natural that the grain size of ZGRO in Rh<sub>2</sub>O<sub>3</sub>/ZGRO increased during the calcination at 500 °C for 1 h. In addition, the surface area decreased to 44.1 m<sup>2</sup>/g (Rh<sub>2</sub>O<sub>3</sub>/ZGRO) from 153 m<sup>2</sup>/g (as-prepared ZGRO).

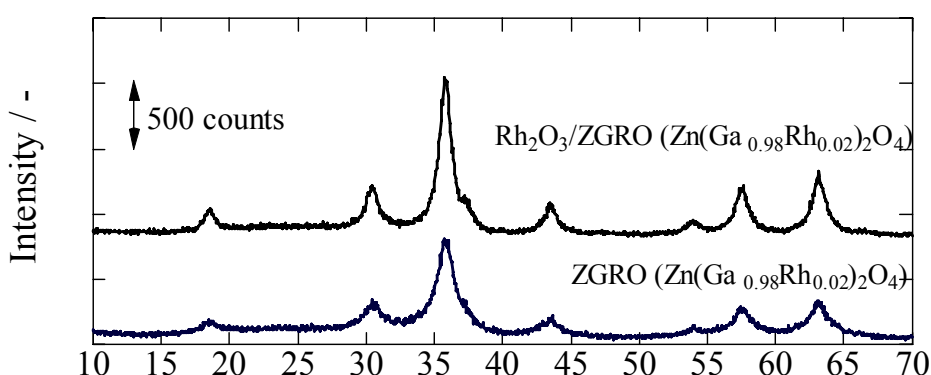


Figure S3. X-ray powder diffraction patterns of as-prepared ZGRO and Rh<sub>2</sub>O<sub>3</sub>/ZGRO powders.

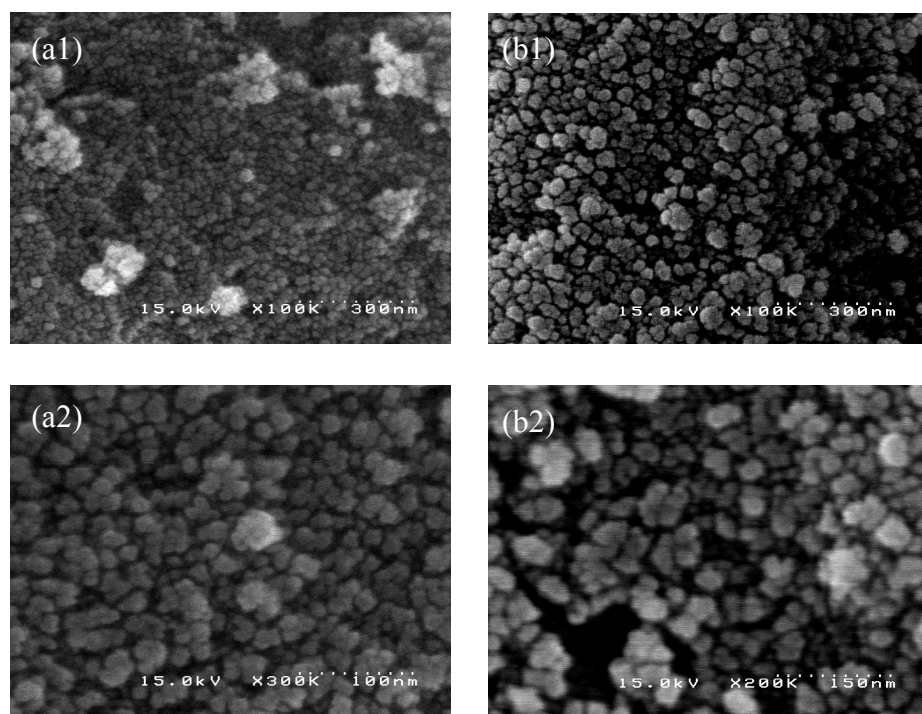


Figure S4. SEM images of as-prepared ZGRO (a1, a2) and Rh<sub>2</sub>O<sub>3</sub>/ZGRO (b1, b2). Note that the magnifications of a1 and b1 are identical, whereas a2 is of higher magnification than b2.

### ESI-7) Additional explanations for the band structure of ZGRO

As described in the main text, we concluded that the introduced Rh formed isolated narrow bands composed of Rh  $t_{2g}^6$  and  $e_g^0$  within the forbidden band of ZnGaO<sub>4</sub>. This conclusion is inconsistent with the DOS calculation in Fig. 1b in that Rh  $e_g^0$  appeared to mix with the CB of ZnGaO<sub>4</sub>. We consider that this inconsistency was likely because of the small value of x (0.02) in Zn(Ga<sub>1-x</sub>Rh<sub>x</sub>)<sub>2</sub>O<sub>4</sub> for the prepared composition, compared to the value used for the calculated composition (x = 0.25). Thus, it can be considered that Rh  $e_g^0$  did not mix with the CB of ZnGaO<sub>4</sub>, rather, it formed the isolated narrow band in the forbidden band below the CB.

### ESI-8) Wavelength distribution of the irradiated light (Fig. S5).

Wavelength distributions of the irradiated lights are shown in Fig. S5. As the light intensities were unknown due to the specifications of the spectroradiometer (USR-30, Ushio), the R-axis was drawn using arbitrary units.

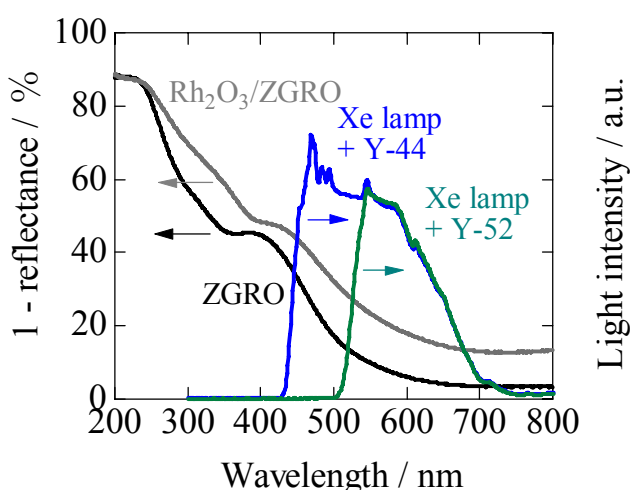


Figure S5. Wavelength distributions of the irradiated light are shown. The light intensities are unknown due to the specifications of the spectroradiometer (USR-30, Ushio), however, that is estimated to be ca. 50 mW/cm<sup>2</sup> (Xe lamp + Y44 glass filter). UV-visible absorption spectra of bare ZGRO, Rh<sub>2</sub>O<sub>3</sub>/ZGRO are also shown.

The apparent quantum efficiency (QE) was calculated to be ca. 0.013 % by utilizing the incident light intensity of 50 mW/cm<sup>2</sup> (estimated value, Xe lamp + Y-44 glass filter) and the following equation, the apparent QE (%) = {(number of evolved H<sub>2</sub> molecules × 2) / number of incident photons} × 100 (after ref. 2, K. Maeda, K. Teramura, T. Takata, M. Hara, N. Saito, K. Toda, Y. Inoue, H. Kobayashi and K. Domen, *J. Phys. Chem. B*, 2005, **109**, 20504-20510).

### ESI-9) Additional explanation for the H<sub>2</sub> evolution activity in the presence of Rh<sub>2</sub>O<sub>3</sub>/ZGRO.

H<sub>2</sub> evolution gradually decreased with increasing repetition times, which may have been due to the detachment of grafted Rh<sub>2</sub>O<sub>3</sub> from ZGRO. However, it is possible that the detachment of Rh<sub>2</sub>O<sub>3</sub> from ZGRO stopped from the 4th to 5th cycle because the H<sub>2</sub> evolution increased.

### ESI-10) Details for the estimation of the turnover number

Sixty mg of the Rh<sub>2</sub>O<sub>3</sub>/ZGRO sample was used for water splitting tests. The present Rh<sub>2</sub>O<sub>3</sub>/ZGRO sample contained Rh<sub>2</sub>O<sub>3</sub> with a Rh<sub>2</sub>O<sub>3</sub>/ZGRO weight percentage of 0.5 wt%. Therefore, the weight of Rh<sub>2</sub>O<sub>3</sub> was 0.3 mg, which corresponds to 1.2 μmol. We confirmed that the total amount of H<sub>2</sub> generation was 4.7 μmol. Thus, the turnover number of produced H<sub>2</sub> to the total amount of co-catalyst Rh<sub>2</sub>O<sub>3</sub> was 4.7 μmol / 1.2 μmol, equalling 3.9.

### ESI-11) Preliminary experiments for the H<sub>2</sub> evolution in the presence of photocatalysts obtained by the solid state reaction (Fig. S6 and Fig. S7).

Not shown here, but XRD patterns indicated that ZGRO (SSR), ZGO and ZRO obtained by the solid state reaction maintained a cubic crystal system with homogeneous spinel  $ZnGa_2O_4$  crystallinity. The BET surface area of ZGRO (SSR) was  $2.36\text{ m}^2/\text{g}$ , which is much smaller than the surface area ( $153\text{ m}^2/\text{g}$ ) prepared by the hydrothermal method. In Fig. S6a, the UV-visible absorption spectra of ZGRO (SSR), ZGO and ZRO are shown. The spectrum of ZGRO (SSR) was quite similar to that of ZGRO. In Fig. S6b, the UV-visible absorption spectra of  $Rh_2O_3/ZGRO$  (SSR) is also shown.

We performed the preliminary experiments to evaluate the H<sub>2</sub> evolutions using  $Rh_2O_3/ZGRO$  (SSR),  $Rh_2O_3/ZGO$  and  $Rh_2O_3/ZRO$  in the presence of CH<sub>3</sub>OH under visible light irradiation with wavelengths of  $> 420\text{ nm}$  (Fig. S7). With respect to  $Rh_2O_3/ZGO$  and  $Rh_2O_3/ZRO$ , low levels of H<sub>2</sub> evolution were generated, however  $Rh_2O_3/ZGRO$  (SSR) produced H<sub>2</sub> at higher rate. So, we can confidently conclude that the introduced Rh<sup>3+</sup>, which forms the midgap states originated from fully occupied t<sub>2g</sub><sup>6</sup> and empty e<sub>g</sub><sup>0</sup>, plays a role in the visible light sensitivity observed in this study. It should be noted that that  $Rh_2O_3/ZGRO$  produced H<sub>2</sub> at much higher rate than  $Rh_2O_3/ZGRO$  (SSR).

In addition, the UV-visible absorption spectrum of  $Rh_2O_3/ZGRO$  (SSR) after visible light irradiation with wavelength of  $> 420\text{ nm}$  in the presence of CH<sub>3</sub>OH was almost the same as that of  $Rh_2O_3/ZGRO$  (SSR) before light irradiation (Fig. S6b). This tendency is different from the observation in Rh-doped SrTiO<sub>3</sub> (STRO) in ref. 3 (R. Konta, T. Ishii, H. Kato and A. Kudo, *J. Phys. Chem. B*, 2004, **108**, 8992-8995). According to Kudo et al, the UV-visible absorption spectra of STRO (introduction of Rh at Ti<sup>4+</sup> site) before and after photocatalytic water-splitting reaction were drastically changed. They considered the existence of two different species of Rh at least in as-prepared STRO. Those were Rh<sup>3+</sup> and a Rh species with a higher oxidation number than Rh<sup>3+</sup> such as Rh<sup>5+</sup> due to the charge compensation. Then, the Rh with higher oxidation number easily reduced to Rh<sup>3+</sup> by photogenerated electrons at an early stage of the water-splitting reaction, indicating that the Rh with higher oxidation number worked as an electron acceptor. In contrast, as for our sample, ZGRO, Rh was introduced at Ga<sup>3+</sup> site and thus, it is probable that Rh existed as Rh<sup>3+</sup> in as-prepared ZGRO. Then, the Rh in ZGRO did not act as an electron acceptor under visible light irradiation.

It is sure that the Rh<sub>eg</sub><sup>0</sup> state contributes to the band structure (especially to the CB) of STRO. As is well known, the CB of STO is composed of Ti 3d. In contrast, the CB of ZGO is composed of mainly Zn 4s. The energy of Ti 3d in STO is lower than those of Zn 4s in ZGO. In fact, the CB bottom energy of STO is lower than that of ZGO (if we discuss using the potential, the CB bottom potential of STO is more positive (-0.2 V vs. SHE) than that of ZGO (-1.2 V vs. SHE)). Then, we might possibly speculate that Ti 3d is energetically comparable to the Rh<sub>eg</sub><sup>0</sup> state and that Ti 3d might electronically overlap with Rh<sub>eg</sub><sup>0</sup>, forming the CB of STRO. So, our speculation does not essentially conflict with the conclusion drawn by Kudo et al. In contrast, Zn 4s did not electronically overlap with the Rh<sub>eg</sub><sup>0</sup> state, forming the isolated Rh<sub>eg</sub><sup>0</sup> state below the CB.

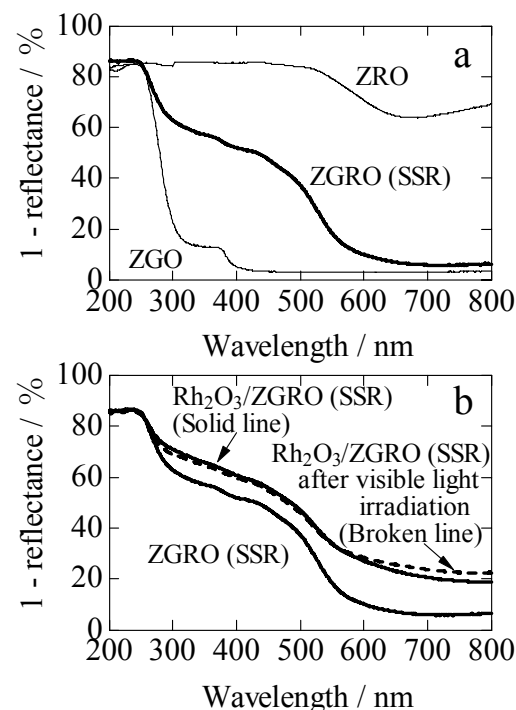


Figure S6. UV-visible absorption spectra of ZGRO (SSR), ZGO and ZRO obtained by the solid state reaction (a). UV-visible absorption spectra of bare ZGRO (SSR),  $Rh_2O_3/ZGRO$  (SSR) and  $Rh_2O_3/ZGRO$  (SSR) after visible light irradiation with wavelengths of  $> 420\text{ nm}$  in the presence of CH<sub>3</sub>OH (b).

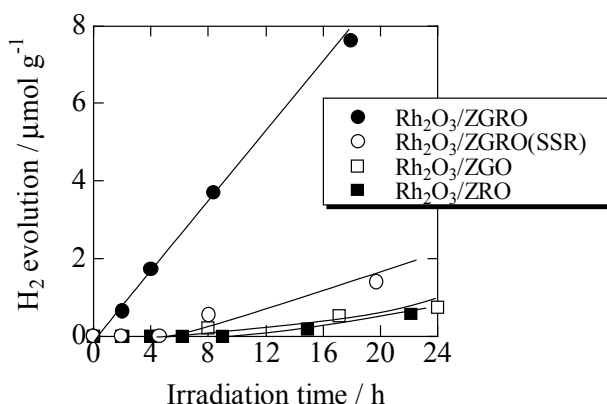


Figure S7. Changes in H<sub>2</sub> concentration by water splitting as a function of time in the presence of  $Rh_2O_3/ZGRO$  (SSR),  $Rh_2O_3/ZGO$  and  $Rh_2O_3/ZRO$  photocatalysts under visible-light irradiation at  $> 420\text{ nm}$ . CH<sub>3</sub>OH was added as sacrificial agent. H<sub>2</sub> concentration change in the presence of  $Rh_2O_3/ZGRO$  is also shown (the same as the first cycle in Fig. 2 (a)).